

FMRI DATA AUGMENTATION VIA SYNTHESIS

Peiye Zhuang¹ Alexander G. Schwing² Oluwasanmi Koyejo^{1,3}

University of Illinois at Urbana-Champaign

¹Dept. of Computer Science, ²Dept. of Electrical and Computer Engineering, ³Beckman Institute
{peiye, aschwing, sanmi}@illinois.edu

ABSTRACT

We present an empirical evaluation of fMRI data augmentation via synthesis. For synthesis we use generative models trained on real neuroimaging data to produce novel task-dependent functional brain images. Analyzed generative models include classic approaches such as the Gaussian mixture model (GMM), and modern implicit generative models such as the generative adversarial network (GAN) and the variational autoencoder (VAE). In particular, the proposed GAN and VAE models utilize 3-dimensional convolutions, which enables modeling of high-dimensional brain image tensors with structured spatial correlations. The synthesized datasets are then used to augment classifiers designed to predict cognitive and behavioural outcomes. Our results suggest that the proposed models are able to generate high-quality synthetic brain images which are diverse and task-dependent. Perhaps most importantly, the performance improvements of data augmentation via synthesis are shown to be complementary to the choice of the predictive model. Thus, our results suggest that data augmentation via synthesis is a promising approach to address the limited availability of fMRI data, and to improve the quality of predictive fMRI models.

Index Terms— fMRI generation, GANs, VAEs, GMMs

1. INTRODUCTION

Progress in computational cognitive neuroimaging research is stifled by the difficulty of obtaining large quantities of brain imaging data [1]. This is especially apparent in *decoding* studies where machine learning methods are used to predict cognitive and behavioral outcomes of brain imaging experiments [2]. To this end, research has focused on increasingly sophisticated predictive models that can take advantage of specialized properties of brain images [3, 4, 5]. Our work is motivated by the view that generative models provide another useful tool for improving the performance of brain decoding models via data augmentation, and furthermore, that synthesis-based data augmentation is complementary to advances in classification models. Indeed, data augmentation is a standard approach in computer vision [6], where it has been shown to improve the performance of predictive models. Classic data augmentation is focused on linear transformations such as rota-

tion and scaling, and nonlinear methods such as adding noise. More recently, implicit generative models have been proposed to capture rich notions of natural variability [7].

Inspired by this progress, our work seeks to answer: *Can data augmentation using generative models be used to improve fMRI classification performance?* This manuscript provides – to our knowledge for the first time, affirmative results suggesting that it is indeed possible to generate artificial, high-quality, diverse, and task-dependent functional brain images. Furthermore, we provide empirical evidence that the synthesized data can be used for data augmentation – resulting in improved fMRI classifier performance. To better understand fMRI data augmentation we provide results for Gaussian mixture models (GMMs), variational auto-encoders (VAEs) and generative adversarial nets (GANs). In addition to qualitative evaluation, we show quantitative results demonstrating that classifiers trained using the generated images combined with real images result in improved performance as compared to classifiers trained only with real images.

2. BACKGROUND AND RELATED WORK

Deep neural networks have been used for classifying brain imaging data [8, 9, 5, 10]. Our approach differs in that we will use generative models to obtain artificial fMRI data. We assume the reader to be familiar with GMMs and review only briefly VAEs and GANs in the following.

Variational auto-encoders (VAEs): VAEs aim to maximize the parametric likelihood $p_\theta(\mathbf{x})$, where \mathbf{x} is a sample from a dataset. To this end, a low-dimensional space represented by variable \mathbf{z} is hypothesized and one optimizes the lower bound

$$\log p_\theta(\mathbf{x}) \geq -\text{KL}(q_\phi(\mathbf{z}|\mathbf{x}), p(\mathbf{z})) + \mathbb{E}_{q_\phi(\mathbf{z}|\mathbf{x})}[\log p_\theta(\mathbf{x}|\mathbf{z})],$$

which compares the approximate posterior q_ϕ to the prior $p(\mathbf{z})$ using the KL-divergence, while simultaneously estimating reconstruction via the decoding $p_\theta(\mathbf{x}|\mathbf{z})$.

Generative adversarial nets (GANs): To learn a distribution over data \mathbf{x} , a GAN [11] formulates a 2-player non-cooperative game between two deep nets: (1) the generator G which depends on a random noise vector \mathbf{z} sampled from a known prior

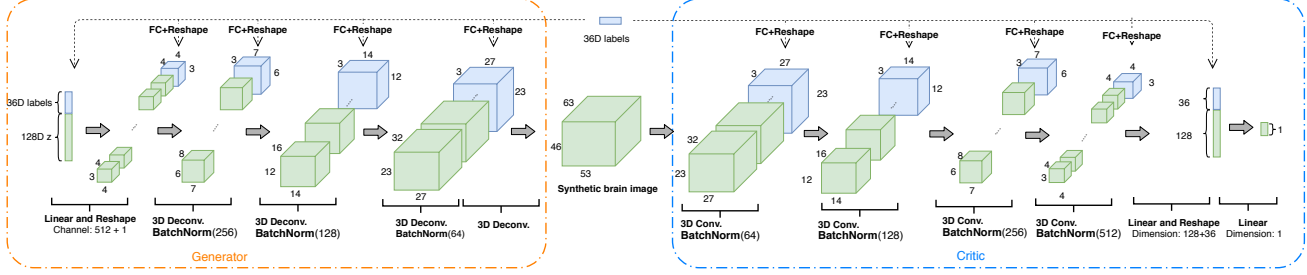


Fig. 1: ICW-GAN architecture. For the generator (orange box), the 128-dimensional encoding z is drawn from a multivariate Gaussian. The label vector is a binary encoding. It is concatenated to input and hidden layers, and for each of the 4 layers, fully connected layers followed by a tanh activation transform the label vector to volumes of appropriate size. The structure of the discriminator (blue box) is a mirrored generator.

distribution P_z and produces an image $G_\theta(z)$; (2) the discriminator D which receives synthetic or real data, and is trained to differentiate as accurately as possible. Since the generator is tasked to make differentiation as hard as possible the resulting formulation is a saddle-point objective.

Many formulations have been proposed to improve upon the original idea [12]. Here, we use the Improved Wasserstein GAN (IW-GAN) framework [13] which optimizes w.r.t. parameters θ and w

$$\mathbb{E}_{z \sim P_z} [D_w(G_\theta(z))] - \mathbb{E}_{x \sim P_r} [D_w(x)] + \lambda \mathbb{E}_{\hat{x} \sim P_{\hat{x}}} [(\|\nabla_{\hat{x}} D_w(\hat{x})\|_2 - 1)^2], \quad (1)$$

where P_r is the real data distribution, \hat{x} is a convex combination of real data and artificial samples, i.e., $\hat{x} \leftarrow \epsilon x + (1 - \epsilon)G_\theta(z)$ with ϵ drawn from a uniform distribution ($\epsilon \sim U[0, 1]$), and λ is a gradient penalty coefficient.

3D-GANs [14] extend GANs to 3D object generation. Different from classical GANs, 3D-GANs apply 3-dimensional convolutions in both the generator and the discriminator. By learning deep object representations, 3D GANs can generate visually appealing yet variable 3D object volumes. We use conditional variants of both VAEs and GANs [15, 16].

3. APPROACH

We use a GMM to directly model the high-dimensional data likelihood, using the expectation-maximization (EM) algorithm to learn parameters of the Gaussian distributions from training data. We slightly adjust conditional VAEs (CVAEs) and GANs as discussed subsequently: for CVAEs, we use 3-dimensional convolutions which enable modeling of the spatial relation within high-dimensional brain images. We modify GANs in a similar way and discuss our adjustments for an improved conditional Wasserstein GAN (ICW-GAN) briefly.

Similar to classical GANs, ICW-GANs are formulated as a non-cooperative two-player game between two adversaries: a generator G_θ and a discriminator D_w .

Different from classical GANs, 3D convolution and deconvolution are used to capture the spatial structure of the voxel information. Moreover, both the discriminator D_w and the generator G_θ are conditioned on available labels. We also use

the Wasserstein distance and gradient penalty [13] in the objective function. As a result, our ICW-GAN integrates 3D-GANs, conditional GANs and IW-GANs.

The overall model architecture is illustrated in Fig. 1. Our generator consists of 4 fully convolutional layers, batch normalization, ReLU layers added in between, and a sigmoid layer at the end. The discriminator architecture is a mirrored generator except for the final layer which uses a linear activation. To include label information, we concatenate labels to the input and hidden layers. We note in passing that we experimented with concatenating labels in various layers and did not observe significant differences. Thus, we chose to implement the model using full concatenation of labels.

The objective function of the ICW-GAN model is

$$L = \mathbb{E}_{z \sim P_z} [D_w(G_\theta(z|y))] - \mathbb{E}_{x \sim P_r} [D_w(x|y)] + \lambda \mathbb{E}_{\hat{x} \sim P_{\hat{x}}} [(\|\nabla_{\hat{x}} D_w(\hat{x}|y)\|_2 - 1)^2].$$

Downstream Classifiers We consider classification with data augmentation to quantitatively investigate the hypothesis that the generated images accurately reproduce the conditional image statistics. We note that support vector machines (SVMs) and deep neural net classifiers are state of the art for fMRI applications [4] and we consider it sufficient to employ them for evaluation. To this end, we compare the SVM and the 3D deep net classifier trained with real brain images (‘Real’) or real plus synthetic brain images (‘Real+Synth.’). Accuracy, macro F1, precision, and recall metrics are used to measure the results.

SVM: As is common for fMRI data, we train a simple linear SVM on masked training data to classify the masked test data. By applying the computed mask to a brain volume, invalid voxels are discarded and valid voxels are placed in a 1-dimensional vector, thus reducing the dimension of the brain volumes. The mask is computed based on the training data. Several strategies of mask computation can be used, e.g., computing the mask corresponding to gray matter part of the brain or computing the mask of the background from the image border. We conduct the experiments on several masking strategies and do not find much difference.

Table 1: Classification results for collection 1952.

Input	Gen. model	Classifier	Accuracy	Macro F1	Precision	Recall
Real	-	SVM	0.8181	0.82	0.8333	0.8133
Real+noise	-	SVM	0.8185	0.82	0.8367	0.82
Real+Synth.	GMM	SVM	0.8188	0.82	0.8366	0.82
Real+Synth.	CVAE	SVM	0.8248	0.8267	0.8367	0.8233
Real+Synth.	ICW-GAN	SVM	0.8311	0.83	0.8433	0.8333
Real	-	DNN	0.852	0.857	0.872	0.8523
Real+noise	-	DNN	0.8581	0.856	0.8719	0.8579
Real+Synth.	GMM	DNN	0.8604	0.8631	0.8749	0.8604
Real+Synth.	CVAE	DNN	0.8684	0.869	0.8827	0.8683
Real+Synth.	ICW-GAN	DNN	0.8799	0.8825	0.8933	0.88

Table 2: Classification results for collection 2138.

Input	Gen. model	Classifier	Accuracy	Macro F1	Precision	Recall
Real	-	SVM	0.6234	0.5967	0.6	0.6233
Real+noise	-	SVM	0.6348	0.6133	0.61	0.6367
Real+Synth.	GMM	SVM	0.6385	0.6	0.6033	0.6333
Real+Synth.	CVAE	SVM	0.6428	0.62	0.6233	0.6397
Real+Synth.	ICW-GAN	SVM	0.6404	0.62	0.6267	0.64
Real	-	DNN	0.7028	0.6939	0.7162	0.7029
Real+noise	-	DNN	0.7353	0.723	0.7373	0.7353
Real+Synth.	GMM	DNN	0.7393	0.723	0.7303	0.7393
Real+Synth.	CVAE	DNN	0.7503	0.738	0.7533	0.7503
Real+Synth.	ICW-GAN	DNN	0.7494	0.7393	0.759	0.7493

Deep Neural Net: The deep neural net structure is similar to the discriminator with a 3-dimensional structure and an identical number of convolution layers with Leaky ReLU activations. Unlike the discriminator, the classifier obviously does not concatenate intermediate and input data with any label information.

4. DATA AUGMENTATION ANALYSIS

In this section we quantitatively and qualitatively analyze the proposed techniques, shedding light on data augmentation for fMRI data. First, we present quantitative results for 3D volume classification via training of downstream classifiers on mixtures of real and synthetic data. We further employ as data augmentation methods a Gaussian Mixture Model (GMM), a CVAE, and an ICW-GAN. A stratified 3-fold cross validation is leveraged for all experiments which means that we maintain the percentage of brain images for each class in each fold. We conduct each classification experiment three times and average the results in order to improve statistical reliability. We will also present detailed qualitative results via examples of generated 3D volumes.

Neurovault [17] is currently the largest open database of preprocessed neuroimaging data (particularly focused on cognitive neuroscience). We evaluate the performance of the generative methods on the two large Neurovault functional brain image collections 1952 and 2138 which are publicly available. In the preprocessing step, we apply min-max normalization on the brain images to a 0-1 range.

Dataset 1 (Collection 1952) results: Collection 1952 is obtained from OpenfMRI, the Human Connectome Project, and the Neurospin research center. The dimensions of the brain im-

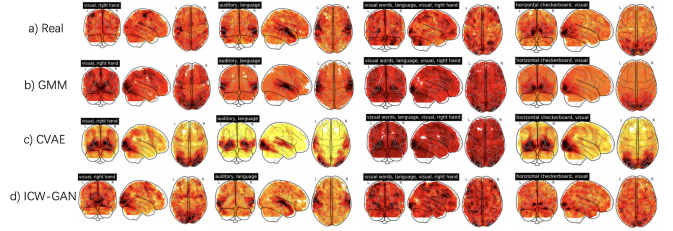


Fig. 2: Real and synthetic data of collection 1952. Each row shows brain images, either real or synthetic data generated by GMM, CVAE and ICW-GAN. Each column presents the brain images of the same class. Classes from left to right: ‘visual, right hand’, ‘auditory, language’, ‘visual words, language, visual, right hand’, and ‘horizontal checkerboard, visual’.

ages in collection 1952 are $53 \times 63 \times 46$. Containing 6573 brain images and 45 classes with a total number of 19 sub-classes, e.g., a multi-label encoding, collection 1952 is designed to map a wide set of cognitive functions. The labels are the set of cognitive processes associated with the image, e.g., ‘visual,’ ‘language,’ and ‘calculate.’ Over the dataset, classes with more than 100 images are split into training, validation and test subsets with a ratio 7:1:2. For classes with less than 100 images but more than 30 samples, we use a 3:1:2 data split. Nine classes with less than 30 samples are ignored. This leaves 4375, 675, and 1398 training, validation, and test brain images, including a total of 36 classes with at least 30 examples. A one-hot encoding is applied to the 36 classes.

We employ a data augmentation method and the generative models mentioned above on collection 1952. Recall that the original brain images are normalized to the 0-1 range. Thus we choose to test Gaussian noise with a mean value of 0 and a variance of 0.01 as data augmentation. We also experimented with variances of 0.01, 0.05, 0.1 and 0.3 and observed that augmentation performed best with a variance of 0.01 which we refer to as ‘Real+noise.’ We train a separate Gaussian Model for each label. When synthesizing a new image, we first choose a specific class and then randomly sample from the trained GMM. We train the CVAE and the ICW-GAN with a batch size of 50, optimized by an Adam Optimizer with an initial learning rate of $1e-4$ until convergence. The dimension of the latent variables in the CVAE is 128. Only one CVAE and one ICW-GAN model are trained for collection 1952.

To further assess the quality of the generated data, we evaluate the performance of downstream classifiers. To train the classifiers we use either real data, real data plus 100 real data with additive Gaussian noise per class, or real data plus 100 generated data per class. Note that the test data for classification is always composed of real images. The classification results are shown in Table 1. The first column indicates the type of training data we use for the classifier. The second column represents the generative source of the synthetic data. The third column denotes the classifier type, i.e., an SVM or a deep neural net (‘DNN’). We use the validation dataset to choose the best training models and use these models to

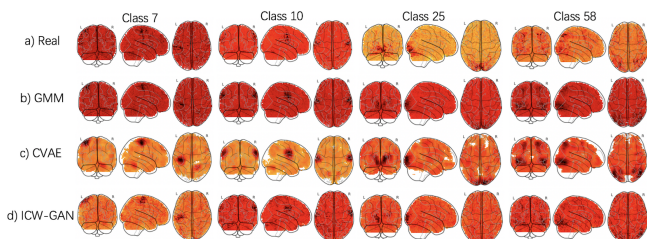


Fig. 3: Real and synthetic data of collection 2138. Each row shows the brain images from real or synthetic data generated by GMM, CVAE and ICW-GAN. The brain images in each column have the same class label.

classify the test data. We observe that including the synthetic data is generally beneficial for classifier training.

Dataset 2 (Collection 2138) results: Collection 2138 includes data from the Individual Brain Charting (IBC) project, developed to collect high resolution fMRI of 12 subjects that undergo a large number of tasks: the HCP tasks, the ARCHI tasks, a specific language task, video watching, low-level visual stimulation, etc. There are 1847 brain images, 61 classes and 50 labels in collection 2138. The labels are encoded with a one-hot scheme. Because of the small size of the dataset, we randomly choose 70% of the brain images as training data and leave 30% as test data. The dimension of brain images in collection 2138 is $105 \times 126 \times 91$, which is relatively large; thus we downsample¹ the brain images to $53 \times 63 \times 46$. Similar to the experiments on collection 1952, we apply simple data augmentation and generative methods, followed by downstream classifiers. The dimension of the latent variables in the CVAE is 32. The input of the classifiers can be only real data, real data plus 20 real data with additive Gaussian noise per class, or real data plus 20 generative data per class. The classification results are summarized in Table 2.

Again we observe that usage of synthetic data is generally beneficial for classifier training. Furthermore, the deep neural network generative models – the CVAE and the ICW-GAN, can significantly outperform the addition of noise and the GMMs for classification. Besides, we also observe that the deep net classifier generally outperforms linear SVMs.

Visualization of synthetic images: 2D projections of several real and synthetic brain volumes of collection 1952 and collection 2138 are illustrated in Fig. 2 and Fig. 3. The voxels of the volumes are normalized to $[0, 1]$. The dark areas in the projections represent high voxel intensities, i.e., significant activity. The projections in Fig. 2 are real and synthesized brain images conditioned on the accompanying cognitive process labels shown on the top left. The classes in Fig. 3 represent types of the tasks received by the subjects (Class 7: ‘response execution’, ‘right finger response execution’; Class 10: ‘response

¹Downsampling and parcellation are common practices in fMRI analysis, as standard preprocessing renders fMRI images to be spatially smooth [18]. In addition, there is significant evidence in the fMRI literature that downsampling has limited effect on classifier performance (particularly cross-subject brain alignment and subsequent smoothing, see Figure 3 of [19]). This is not necessarily true for other kinds of brain imaging. For example, structural brain images can be reliably analyzed at higher resolution.

Table 3: Variances for 3-fold cross validation on data 1952.

Input	Gen. model	Classifier	Accuracy	Macro F1	Precision	Recall
Real	-	SVM	2.8e-4	3.0e-4	4.3e-4	4.3e-4
Real+noise	-	SVM	6.8e-5	1.0e-4	4.4e-5	1.0e-4
Real+Synth.	GMM	SVM	3.1e-4	4.0e-4	2.3e-4	4.0e-4
Real+Synth.	CVAE	SVM	7.5e-5	1.3e-4	1.3e-4	3.3e-5
Real+Synth.	ICW-GAN	SVM	2.9e-4	3.0e-4	1.3e-4	4.3e-4
Real	-	DNN	2.8e-4	3.1e-4	3.3e-4	2.8e-4
Real+noise	-	DNN	2.5e-4	2.4e-4	2.4e-4	2.5e-4
Real+Synth.	GMM	DNN	3.3e-5	3.1e-5	2.2e-5	3.4e-5
Real+Synth.	CVAE	DNN	1.5e-5	2.3e-6	1.4e-5	1.4e-5
Real+Synth.	ICW-GAN	DNN	1.3e-4	9.0e-5	3.0e-5	1.4e-4

execution’, ‘tongue response execution’; Class 25: ‘response execution’, ‘working memory’, ‘place maintenance’, ‘visual place recognition’; Class 58: ‘working memory’, ‘string maintenance’, ‘visual string recognition’). We observe that the generative models accurately learn active regions for the both datasets. Visual examination of the generated images by neuroscience experts suggests high quality and high diversity. In particular, experts report high activation in the appropriate brain regions, e.g., the motor cortex for motor labels, and the visual cortex for visual labels.

Variance of cross-validated performance in ICW-GAN:

We test our model in various cross-validation settings and calculate the mean variance of the evaluation metrics over the three folds (Table 3) on collection 1952. The small variances suggest that the reported accuracy differences are indeed statistically significant.

5. CONCLUSION

The results of this manuscript compare – to our knowledge for the first time, the performance of different generative models trained on brain imaging data for data augmentation. In our experiments, 3D generative models, particularly the conditional VAE and the ICW-GAN, are shown to generate high quality, diverse, and task dependent brain images. Beyond qualitative evaluation, we evaluate quantitative performance by using the generated images as additional training data in a predictive model – mixing synthetic and real data to train classifiers. The results show that our synthetic data augmentation can improve classification accuracy. The ICW-GAN and the CVAE easily outperform the generative baselines of GMMs and data augmentation with Gaussian noise, which illustrates that not all data augmentation methods are equally beneficial for the task of image generation. We hope our results inspire additional research on generative models for brain imaging data. Future work will focus on additional qualitative evaluation of the generated images by neuroscience experts and exploration of additional applications. We also plan to more thoroughly investigate the trained models to explore what they may contribute to the science of individual variability in neuroimaging. Finally, we plan to expand our models to combine data across multiple studies – each of which use different labels, by exploring techniques for merging labels based on the underlying cognitive processes [20].

References

- [1] R. A. Poldrack and K. J. Gorgolewski, "Making big data open: data sharing in neuroimaging," *Nature neuroscience*, 2014.
- [2] G. Varoquaux and B. Thirion, "How machine learning is shaping cognitive neuroimaging," *GigaScience*, 2014.
- [3] D. D Cox and R.-L Savoy, "Functional magnetic resonance imaging (fMRI)"brain reading": detecting and classifying distributed patterns of fMRI activity in human visual cortex," *Neuroimage*, 2003.
- [4] F. Pereira, T. Mitchell, and M. Botvinick, "Machine learning classifiers and fMRI: a tutorial overview," *Neuroimage*, 2009.
- [5] D. D. Nathawani, T. Sharma, and Y. Yang, "Neuroscience meets deep learning," 2016.
- [6] I. Goodfellow, Y. Bengio, and A. Courville, *Deep Learning*, MIT Press, 2016.
- [7] E. Richardson and Y. Weiss, "On gans and gmms," *CoRR*, vol. abs/1805.12462, 2018.
- [8] O. Firat, L. Oztekin, and F. Vural, "Deep learning for brain decoding," in *Image Processing (ICIP), 2014 IEEE International Conference on*, 2014.
- [9] S. Koyamada, Y. Shikauchi, K. Nakae, M. Koyama, and S. Ishii, "Deep learning of fmri big data: a novel approach to subject-transfer decoding," *CoRR*, 2015.
- [10] M. Svanera, S. Benini, G. Raz, T. Hendler, R. Goebel, and G. Valente, "Deep driven fMRI decoding of visual categories," *arXiv preprint arXiv:1701.02133*, 2017.
- [11] I. J. Goodfellow, J. A. Pouget, M. Mirza, B. Xu, D. Warde-Farley, S. Ozair, A. Courville, and Y. Bengio, "Generative Adversarial Nets," in *Advances in neural information processing systems*, 2014.
- [12] M. Arjovsky, S. Chintala, and L. Bottou, "Wasserstein GANs," *arXiv preprint arXiv:1701.07875*, 2017.
- [13] I. Gulrajani, F. Ahmed, M. Arjovsky, V. Dumoulin, and A. Courville, "Improved training of Wasserstein GANs," *Advances in Neural Information Processing Systems*, 2017.
- [14] J. Wu, C. Zhang, T. Xue, B. Freeman, and J. Tenenbaum, "Learning a probabilistic latent space of object shapes via 3d generative-adversarial modeling," in *Advances in Neural Information Processing Systems*, 2016.
- [15] K. Sohn, H. Lee, and X. Yan, "Learning structured output representation using deep conditional generative models," *Advances in Neural Information Processing Systems*, 2015.
- [16] M. Mirza and S. Osindero, "Conditional Generative Adversarial Nets," *arXiv preprint arXiv:1411.1784*, 2014.
- [17] KJ Gorgolewski, G. Varoquaux, G. Rivera, Y. Schwarz, SS Ghosh, C. Maumet, VV. Sochat, T. E-Nichols, Russell A Poldrack, J-B. Poline, et al., "Neurovault. org: a web-based repository for collecting and sharing unthresholded statistical maps of the human brain," *Frontiers in neuroinformatics*, vol. 9, 2015.
- [18] S. Arslan, S. I. Ktena, A. Makropoulos, and et.al, "Human brain mapping: a systematic comparison of parcellation methods for the human cerebral cortex," *NeuroImage*, 2017.
- [19] R. A. Poldrack, D. M. Barch, J. Mitchell, and et.al, "Toward open sharing of task-based fmri data: the openfmri project," *Frontiers in neuroinformatics*, vol. 7, pp. 12, 2013.
- [20] R. A. Poldrack, "Can cognitive processes be inferred from neuroimaging data?," *Trends in cognitive sciences*, 2006.